

Understanding the Resistive Switching Mechanism of 2-D RRAM: Monte Carlo Modeling and a Proposed Application for Reliability Research

Yifu Huang[®], *Graduate Student Member, IEEE*, Yuqian Gu, Yao-Feng Chang, *Member, IEEE*, Ying-Chen Chen[®], *Member, IEEE*, Deji Akinwande[®], *Fellow, IEEE*, and Jack C. Lee, *Fellow, IEEE*

Abstract—The 2-D materials have become promising candidates for resistive random access memory (RRAM) devices as more unique resistive switching (RS) characteristics have recently been revealed. However, endurance is a major challenge for industrialization. Unlike the welldeveloped and recognized conductive filament (CF) model for oxide-based RRAM, the RS mechanism for 2-D RRAM is not well understood. In this article, we first review the dissociation-diffusion-adsorption (DDA) model and the cluster model proposed in previous works on monolayer 2-D RRAM devices. The use of a Monte Carlo (MC) simulator for multilayer 2-D RRAM devices to expand the application of DDA and cluster models is then discussed. A simulator was designed to provide an intuitive physical view by visualizing the stochastic behaviors of the RS process in multilayer 2-D RRAM devices. By comparing the simulated results with experimental data, the endurance characteristic was found to be mainly determined by the formation and collapse of an effective switching layer. We also found that the thickness of the effective switching layer is independent of the total thickness of the multilayer 2-D material and the initial status of the device, which is consistent with the experimental observations. The model and results discussed in this work provide additional insights and guidance for improving the reliability of 2-D RRAM devices.

Index Terms—2-D material, device modeling, Monte Carlo (MC), MoS₂, resistive random access memory (RRAM), resistive switching (RS).

Manuscript received 28 October 2022; revised 27 January 2023; accepted 21 February 2023. Date of publication 6 March 2023; date of current version 24 March 2023. This work was supported in part by the National Science Foundation (NSF) under Grant 1809017, in part by the NSF MRSEC under Cooperative Agreement DMR-1720595, and in part by the NSF NNCI under Award 1542159. The review of this article was arranged by Editor P.-Y. Du. (Corresponding author: Jack C. Lee.)

Yifu Huang, Yuqian Gu, Deji Akinwande, and Jack C. Lee are with the Department of Electrical and Computer Engineering, The University of Texas at Austin, Austin, TX 78712 USA (e-mail: huangyifu@utexas.edu; yuqian@utexas.edu; deji@ece.utexas.edu; leejc@austin.utexas.edu).

Yao-Feng Chang is with Intel Corporation, Hillsboro, OR 97124 USA (e-mail: yao-feng.chang@intel.com).

Ying-Chen Chen is with the School of Informatics, Computing and Cyber Systems and the Center for Materials Interfaces in Research and Applications (¡MIRA!), Northern Arizona University, Flagstaff, AZ 86011 USA (e-mail: Ying-Chen.Chen@nau.edu).

Color versions of one or more figures in this article are available at https://doi.org/10.1109/TED.2023.3249139.

Digital Object Identifier 10.1109/TED.2023.3249139

I. INTRODUCTION

UE to its simple structure, high switching speed, and compatibility with the standard CMOS process, resistive random access memory (RRAM) is extensively studied as a potential technology for artificial intelligence, machine learning, and the Internet of Things [1], [2], [3]. Oxidebased RRAM devices have excellent reliability, and they have been well investigated by researchers over the past few decades [4]. A widely recognized resistive switching (RS) model for oxide-based RRAM is the conductive filament (CF) model [5], where CFs are generated when an external voltage bias is applied to the RRAM device during the SET process. The additional bias needed for SET as-fabricated devices differentiates the first SET, which is referred to as forming. Forming and the SET process are associated with the formation of CFs, during which oxygen vacancies are generated and oxygen ions migrate toward the electrode region, forming percolation-conducting paths [6], [7], [8]: the device transits from a high-resistance state (HRS) to a low-resistance state (LRS). During the RESET process, oxygen ions migrate back to and recombine with oxygen vacancies, leading to the rupture of the CFs and a transition from an LRS to an HRS [9]. The resistance states can be maintained without an external power supply [10]. Therefore, RRAM devices are referred to as nonvolatile resistive switching (NVRS) memory devices [11].

The 2-D materials, including graphene oxide [12], transition metal dichalcogenides (TMDs) [13], [14], and hexagonal boron nitride (h-BN) [15], have attracted much interest for their application to RRAM devices due to their unique mechanical and optical characteristics, extreme thinness, and low power consumption. Our previous work successfully demonstrated universal intrinsic NVRS behaviors in a variety of monolayer TMDs using a vertical metal–insulator–metal (MIM) configuration [16]. The 2-D RRAMs show promising electrical characteristics, including low switching voltages, a high ON/OFF ratio, and forming-free behaviors, which have the potential for use in power-sensitive applications, such as biosensors, and wearable electronics.

0018-9383 © 2023 IEEE. Personal use is permitted, but republication/redistribution requires IEEE permission. See https://www.ieee.org/publications/rights/index.html for more information.

However, low endurance is one of the main barriers to the application of 2-D RRAM [17], [18]. To understand the endurance characteristics of 2-D RRAMs, it is essential to establish models that explain their RS behaviors. In our previous work, a dissociation-diffusion-adsorption (DDA) model was proposed to understand the RS behavior in monolayered MoS₂ [11]. The RS behavior was attributed to reversible Au substitution in MoS₂ sulfur vacancies, which are referred to as conductive points. Furthermore, a cluster model was implemented to explain the failure caused by Au ion clustering in a small region of monolayered MoS₂, which led to excessive high current and Joule heating effects [19]. Our recent work on MoS₂ growth engineering further revealed that the endurance characteristics of 2-D MoS₂ RRAM devices can be largely improved by modifying the thickness of the deposited molybdenum and sulfurization conditions [20].

The origin of the low endurance of 2-D RRAM devices has been shown to come from the stochastic nature of metal ion migration into the 2-D material layer [21], [22], [23]. To provide a better physical picture of the RS and the failure of the multilayer MoS₂ RRAM, we investigate the endurance characteristics of multilayer MoS2-based RRAM devices. We propose a phenomenological percolating model that implements the Monte Carlo (MC) method to simulate the formation and rupture of conductive channels in a MoS₂ layer. Electrothermal simulations are conducted to understand the Joule heating effect that occurs during the RESET process. By comparison with experimental data, the simulation results show that effective switching layers with similar thicknesses appear during iterative RS in RRAM devices with different MoS₂ thicknesses. The collapse of the effective switching layer is shown to lead to device failure. These new insights provide additional guidance for the improvement of MoS₂ RRAM reliability. MoS₂ growth, device fabrication, and the principal electrical characteristics of vertical Au/MoS₂/Au crossbar structure devices [Fig. 1(a)] were reported in our previous work [20].

II. MODEL DESCRIPTION

The model was established based on a vertical MIM-configured MoS₂ RRAM device, as shown in Fig. 1(a). We used e-beam evaporation to deposit 60-nm-thick crossbar electrodes with Au. Fig. 1(b) shows bipolar RS in monolayered MoS2, as described by the DDA model. External voltage bias is applied to the device from the top electrode (TE), and the bottom electrode (BE) is grounded. The overlapped crossbar area defines the device area (2 \times 2 μ m² in this work). A typical current-voltage (I-V) characteristic plot of a multilayer MoS₂ RRAM device is shown in Fig. 1(c). When a positive voltage bias is applied, Au ions with positive charges are driven into the sulfur vacancies by the electric field, leading to a drop in the resistance of the MoS₂ layer. This transition from an HRS to an LRS is commonly referred to as the SET process. As a forming-free device, SET can be triggered without forming process at the beginning of test. Ab initio simulations were conducted to help elucidate the drift of the Au ions. It was found that

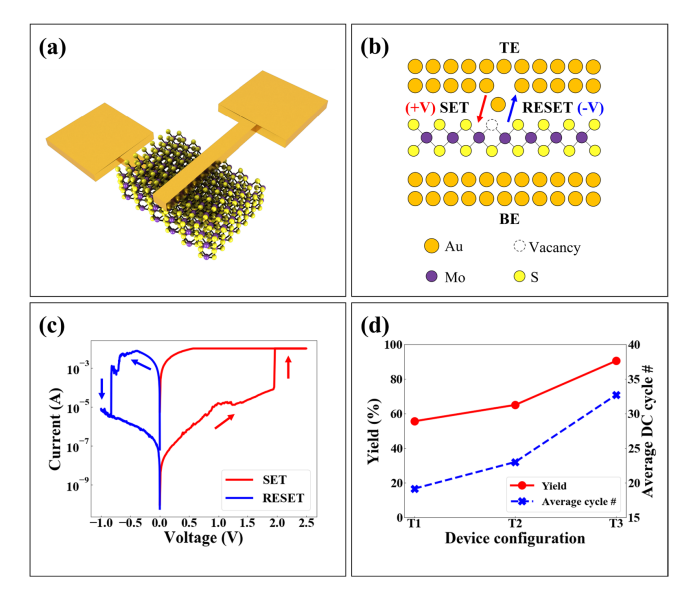


Fig. 1. MoS₂-based vertical MIM configured RRAM device. (a) Schematic of the multilayer MoS₂ RRAM device. (b) Schematic of the DDA model of the RS process. (c) Typical *I–V* plot of the MoS₂ RRAM device RS. (d) Yield and average cycle numbers of multilayer MoS₂ RRAM devices with different MoS₂ thicknesses.

 Au^+ ions are favorable for substitution at sulfur vacancies and increase the density of states around the Fermi level of the MoS_2 , leading to the transition from a semiconducting to a metallic state [24]. During the RESET process, Au ions dissociate from the sulfur vacancies and migrate back to the electrode region by reverse voltage bias at around -0.8 V, where high current (>10 mA) is induced. Both an HRS and an LRS can be maintained without an external power supply, which indicates the NVRS behavior. Stable RS can be achieved at around 100 cycles under dc measurements.

The Joule heating effect plays an important role in the reliability of the transition from an LRS to an HRS. In repeating RS, the vacancy regions in the MoS₂ layer can degrade due to electrical and thermal stress. As a result, large numbers of Au ions accumulate in degraded vacancy regions to form clusters [25]. Exceedingly high current at the clusters creates high-temperature local spots as a result of the Joule heating effect. The failure of the device is attributed to hard breakdowns at these local hotspots. To build a valid model, the experimental data were analyzed statistically. Three different thicknesses of MoS₂, varying from monolayer to trilayer, were used to fabricate the 2-D RRAM devices. In Fig. 1(d), the three different thicknesses of MoS₂ are labeled T1-T3, representing monolayer, bilayer, and trilayer, respectively. The statistical measurements show that both the yield and average dc cycle numbers increase with thicker MoS₂, indicating a positive correlation between reliability and MoS₂ thickness.

The RS caused by the association/dissociation of the Au ions is stochastic; therefore, the random migration behavior of the Au ions must be considered when establishing a descriptive model. The simulation combines the finite-element analysis method and the MC method within a restricted region. The MoS₂ layer is divided into multiple units, defined by the radius of the Au ions (137 pm) [26]. Due to a computation

capability limitation, the simulated area in this work is defined as a 3-D mesh with $20 \times 20 T$ units, where T is the number of simulated layers determined by the MoS₂ thickness. Each simulated unit is initialized as a high-resistance unit (HRU). When an Au ion migrates into a unit, it turns into a low-resistance unit (LRU). The resistance values for the LRU and HRU are estimated by the resistance states determined by the experimental and actual device dimensions. In the simulation, both the SET and RESET processes require multiple steps, reflecting the evolving distribution of the LRUs and the HRUs. At each step, the program traverses all the LRUs and calculates the probability of Au-ion migration based on the distribution of the LRUs within the simulated area. The MC method is used to determine the movement of the LRUs in the next step. Therefore, an updated map for the simulated area is generated after each step. When the SET process is finished, a cluster judgment algorithm is implemented to decide whether the device has failed. The general flowchart of the simulation process is shown in Fig. 2(d). The algorithms for the SET, RESET, and cluster judgment are discussed in more detail in the following sections.

A. SET Algorithm

During the SET process, the migration of Au ions through the MoS_2 layer is considered to be driven by local current density estimated by tunneling [27], which was also adopted in other physics-based MC simulators [28], [29]. The distribution of HRUs and LRUs evolves dynamically in each simulation step. The following assumptions were made to develop the phenomenological simulation.

- The generation of an LRU must come from a nearby LRU.
- The LRU percolation direction is vertical, moving from the TE to the BE. There are no horizontal or diagonal percolations.
- 3) When at least one LRU percolation path reaches the BE and the resistance of the device is lower than the LRS threshold, the SET process stops.

 $P_{\rm SET}$, the probability of an individual LRU migrating to the next unit, is qualitatively estimated by the following equation:

$$P_{\text{SET}} = p_{s_0} + \left(1 - p_{s_0}\right) \cdot \exp\left(-\frac{d}{D}\right) \tag{1}$$

where d is the distance between the lowest LRU and the BE in each of the 20×20 columns at the current state, D is the initial penetration depth of the LRS units, and p_{s0} is the base diffusion possibility. This equation correlates the probability of SET in an individual unit with the current position of the percolation path and the MoS₂ thickness. $P_{\rm SET}$ has a nonzero initial migration probability when d=D, which can be adjusted by the value of p_{s0} to fit the experimental behavior of the device. As the percolation path approaches the BE (decreasing d), the value of $\exp(-d/D)$ increases, reflecting the increasing current resulting from the narrowing tunneling barrier. When d=0, $P_{\rm SET}$ equals 1, which represents the percolation path reaching the BE when the migration of Au toward the BE becomes certain. The SET algorithm flowchart

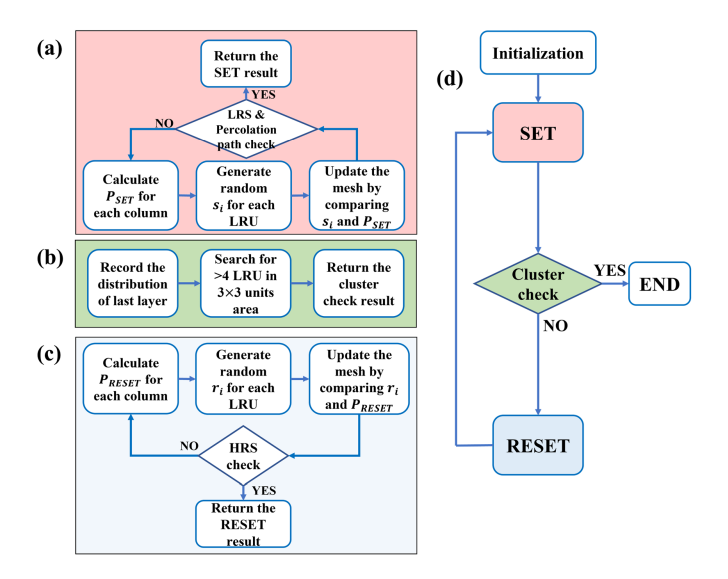


Fig. 2. Flowcharts of the model for RS simulation in 2-D MoS₂ RRAM devices. (a) Flowchart of SET algorithm. (b) Flowchart of cluster check algorithm. (c) Flowchart of RESET algorithm. (d) General flowchart of the simulation process.

is presented in Fig. 2(a). In each step of the SET process, the solver first calculates P_{SET} for each column, which is 400 values. For a single LRU, a random value (s_i) between 0 and 1 is generated to yield a Gaussian distribution, which is compared with P_{SET} . If s_i is larger than P_{SET} , the next unit of the current LRU is marked as low resistance. No new LRU is generated if s_i is smaller than P_{SET} . After visiting all the LRUs, an updated map of the LRUs and HRUs is generated, marking the end of one step in the SET process.

B. RESET Algorithm

The RESET process relies on the Joule heating effect induced by a high current along previously formed lowresistance percolation paths. To study the correlation between the local temperature and the depth of the percolation path, a thermoelectric simulation was conducted using COMSOL Multiphysics. 1 As shown in Fig. 3(a), a 1.5-nm-thick multilayer MoS₂ region with a radius of 10 nm is sandwiched between two 60-nm Au layers. The LRU region is set from $0.1 \times \text{to } 1 \text{ x}$ the thickness of the MoS₂, corresponding to the different resistance states. The temperature distribution is simulated by applying a -1-V external voltage bias [see Fig. 3(b)] using Joule heating equations [6] with electric current (ec) and heat transfer in solids (ht) modules. The highest local temperature occurs in the region of the LRU. The highest temperatures for the different LRU thicknesses are recorded and normalized to fit a function of normalized LRU thickness in the form of (2), as shown in Fig. 3(c)

$$Temp_n = \exp(A \cdot t_n + B) + C \tag{2}$$

$$t_n = \frac{t}{T} \tag{3}$$

where Temp_n is the normalized highest local temperature and A, B, and C are the fitting parameters. The variable t_n is the

¹Registered trademark.

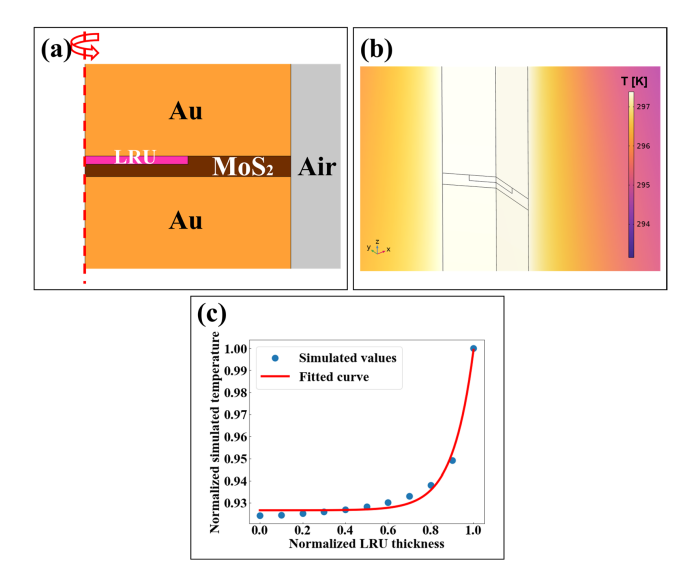


Fig. 3. Finite-element analysis of MoS_2 RRAM device temperature. (a) Schematic of the 2-D axisymmetric simulation. The thickness of the LRU varies from $0.1 \times to 1 x$ the thickness of the MoS_2 . (b) Revolved 3-D simulation of the temperature distribution. (c) Normalized simulated highest temperatures in the MoS_2 RRAM devices with different LRU thicknesses. The red curve is the fit curve for the highest temperature.

normalized LRU thickness, which is equal to the ratio of the LRU thickness (t) to the MoS₂ thickness (T).

The probability of RESET (P_{RESET}) is qualitatively estimated by the following equation:

$$P_{\text{RESET}} = \text{Temp}_n \cdot p_{r0}$$

= $(\exp(A \cdot t_n + B) + C) \cdot p_{r0}$. (4)

In this equation, Temp_n acts as an adjustment parameter that correlates the probability of RESET with the thickness of the LRU. Here, the constant p_{r0} is the base probability of the RESET, which can be adjusted to fit the behavior of the device during the experiments. As shown in Fig. 2(c), similar to the SET process, in each step of the simulated RESET process, the value of P_{RESET} is calculated for each column. Random values between 0 and 1 (r_i) are generated for each LRU and compared with the calculated P_{RESET} to determine the updated LRU and HRU maps based on the following assumptions and rules.

- 1) The LRU will move by one unit from the BE to the TE if the generated r_i is larger than P_{RESET} .
- 2) The LRU will not move if the generated r_i is smaller than P_{RESET} .
- 3) The RESET process stops when the resistance of the device is higher than the HRS threshold.

C. Cluster Judgment Algorithm

The cluster judgment algorithm derived from our previous works [19], [25] is implemented to determine whether an exceedingly high current, which terminates the simulation, occurs in the device. The flowchart for the cluster judgment algorithm is shown in Fig. 2(b). When the simulation of the SET process stops, the distributions of the LRUs and HRUs in the layer adhering to the BE are recorded. The program

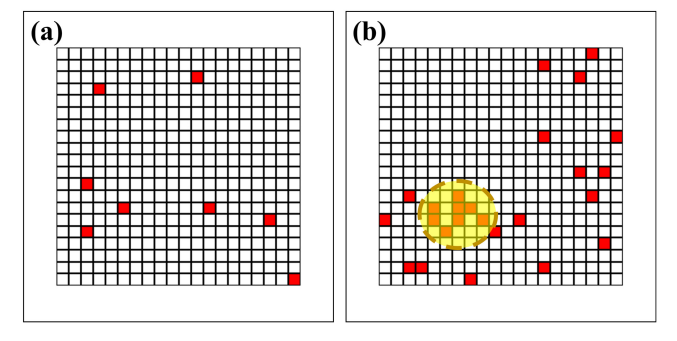


Fig. 4. Typical top-view plots of the final layer adhere to BE in the simulated area. Red boxes are the LRUs. (a) SET process completed without cluster formation. (b) Cluster (yellow circled area) formed after the completion of the SET process.

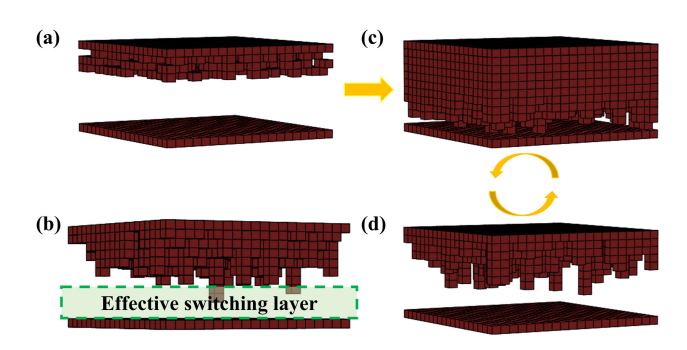


Fig. 5. 3-D simulation of RS in multilayer 2-D MoS₂ RRAM devices. (a) Initial state of the simulation. The red cubes are LRUs that represent Au substitution. Initial LRUs are randomly generated and distributed in the top layers, indicating Au penetration caused by TE deposition. (b) Effective switching layer will appear during the RS process. The device transits between (c) LRS and (d) HRS during the simulation.

then starts to search the Au cluster, defined by a 3×3 unit area with more than four LRUs. The program continues to execute the RESET process and the following RS iterations if no cluster is formed: otherwise, the SET/RESET iteration is terminated when a cluster is detected. Fig. 4(a) shows a typical top-view plot of a cluster-free case final layer, and Fig. 4(b) shows a cluster formed after the iterations.

III. SIMULATION FLOW

Equations (1)–(4) apply to 1-D-to-3-D simulation systems. The choice of dimension should meet the requirements of the problem being investigated. To provide an intuitive physical picture of the failure associated with the formation of conductive clusters, we developed a 3-D model to demonstrate the RS and failure process. As shown in Fig. 5, the model starts by generating the initial state. TE and BE are defined as one layer of LRUs adjacent to the top and bottom of the device area, respectively. In this work, a 3-D mesh with length × width \times thickness equal to $20 \times 20 \times 10$ is deployed as the simulation area to mimic a bilayer MoS₂ RRAM device. Thirty percent of the three layers adjunct to the TE are randomly transformed into LRUs [Fig. 5(a)], representing the penetration of the Au caused by the TE deposition. The initial mesh is imported into the SET process afterward. New LRUs are generated step-by-step in the simulated area following (1) during the SET process. In each step of the SET process, the

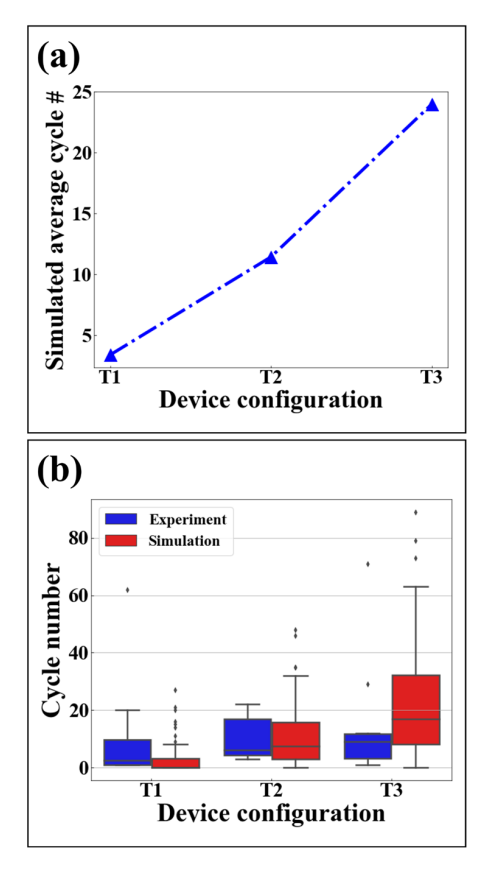


Fig. 6. Endurance simulation results. (a) Simulated average cycle numbers for MoS₂ RRAM devices with different MoS₂ thicknesses. (b) Comparison of the distribution of the experimental and simulation cycle numbers according to the device.

resistance for the entire simulated area is calculated. When at least one percolation path reaches the BE and the device resistance is lower than the LRS threshold, the SET process is terminated. Fig. 5(c) shows the typical status of a simulated device after the SET process. Before starting the RESET process, the last layer of the simulated mesh is extracted and cluster-checked. If no cluster is detected, the simulated mesh after the SET process will continue to go through a step-bystep RESET process, following (2)-(4). The resistance of the simulated device is calculated after each step, ensuring that the program stops when the resistance is beyond the HRS threshold. A typical status plot for a post-RESET device is shown in Fig. 5(d). The completion of the continuous SET and RESET processes is recorded as one cycle. When clusters are detected during the cluster check process, the device is defined as "failed," and the simulation is aborted. The total cycle number is returned after the termination of the simulation.

IV. APPLICATION

To demonstrate the proposed model's capability to simulate 2-D RRAM endurance characteristics for different thicknesses of MoS_2 , we used 5, 10, and 15 unit layers for the T1–T3 device simulations. Following the previously described simulated flow, the devices underwent endurance simulations of 1000 x for a 95% confidence interval. The average cycle numbers were calculated after collecting the simulated endurance

data. The simulated average cycle numbers show the same trend and similar values as those acquired experimentally [see Fig. 6(a)]. However, the simulated cycle number has a wider distribution compared with the experimental data [see Fig. 6(b)]. This is related to the number of devices measured in the experiments being fewer than the number of simulated devices, which added randomness to the experimental data. However, the shared trends between the cycle number and MoS₂ thickness indicate that the simulation program established in this study describes the RS behaviors of the 2-D RRAM devices well and with reasonable precision. The model will be improved by the collection of more experimental data.

In addition, by recording and mapping the simulated area after the RESET finishes, high-resistance regions with similar thicknesses were observed to form during each simulation cycle. This observation is the first time in the research of RS mechanisms of 2-D RRAM and fits our previously proposed qualitative model: increased MoS₂ thickness improves endurance. The layers close to the TE region are occupied by more Au ions under electrical stress during cycling switching. Due to the limitation of the RESET voltage, this region is unlikely to transit to an HRS, leaving the rest of MoS₂ area as an effective switching layer [Fig. 5(b)]. The previously proposed conductive point model can also be applied within this effective switching layer. Moreover, the effective switching layer has a similar thickness compared to the monolayer MoS₂, which is consistent with the similarity of the experimentally observed RS I-V curves of the monolayer and multilayer MoS₂ RRAM devices.

V. CONCLUSION

A phenomenological percolation modeling tool based on an MC algorithm is proposed to simulate the RS behavior of multilayer 2-D RRAM devices. The model helps us obtain a better physical view of the RS mechanisms of multilayer MoS₂. The application of endurance simulation demonstrates the practicality of the model. The observation of a simulated effective switching layer indicates that this model can provide additional insights into the RS mechanism for both multilayer and monolayer MoS₂ RRAM devices. To provide quantitative support for these simulations, future studies should address the Au migration model in 2-D MoS₂.

REFERENCES

- W.-H. Chen et al., "CMOS-integrated memristive non-volatile computing-in-memory for AI edge processors," *Nature Electron.*, vol. 2, pp. 420–428, Aug. 2019.
- [2] H. Jeong and L. Shi, "Memristor devices for neural networks," J. Phys. D, Appl. Phys., vol. 52, no. 2, Jan. 2019, Art. no. 023003.
- [3] K. Sun, J. Chen, and X. Yan, "The future of memristors: Materials engineering and neural networks," *Adv. Funct. Mater.*, vol. 31, no. 8, Feb. 2021, Art. no. 2006773.
- [4] T.-C. Chang, K.-C. Chang, T.-M. Tsai, T.-J. Chu, and S. M. Sze, "Resistance random access memory," *Mater. Today*, vol. 19, no. 5, pp. 254–264, Jun. 2016.
- [5] J. Kang et al., "Oxide-based RRAM: A novel defect-engineering-based implementation for multilevel data storage," in *Proc. 4th IEEE Int. Memory Workshop*, May 2012, pp. 1–4.
- [6] U. Russo, D. Ielmini, C. Cagli, and A. L. Lacaita, "Self-accelerated thermal dissolution model for reset programming in unipolar resistiveswitching memory (RRAM) devices," *IEEE Trans. Electron Devices*, vol. 56, no. 2, pp. 193–200, Feb. 2009.

- [7] Z. Wang et al., "Functional non-volatile memory devices: From fundamentals to photo-tunable properties," *Phys. Status Solidi Rapid Res. Lett.*, vol. 13, no. 5, May 2019, Art. no. 1800644.
- [8] S. C. Chae et al., "Random circuit breaker network model for unipolar resistance switching," *Adv. Mater.*, vol. 20, no. 6, pp. 1154–1159, Mar. 2008.
- [9] S. Aldana et al., "Resistive switching in HfO₂ based valence change memories, a comprehensive 3D kinetic Monte Carlo approach," *J. Phys.* D, Appl. Phys., vol. 53, no. 22, May 2020, Art. no. 225106.
- [10] Y.-C. Chen, H. Li, and W. Zhang, "A novel peripheral circuit for RRAM-based LUT," in *Proc. IEEE Int. Symp. Circuits Syst. (ISCAS)*, May 2012, pp. 1811–1814.
- [11] X. Wu, R. Ge, Y. Huang, D. Akinwande, and J. C. Lee, "Resistance state evolution under constant electric stress on a MoS₂ non-volatile resistive switching device," *RSC Adv.*, vol. 10, no. 69, pp. 42249–42255, 2020.
- [12] S. Ki Hong, J. E. Kim, S. O. Kim, and B. J. Cho, "Analysis on switching mechanism of graphene oxide resistive memory device," *J. Appl. Phys.*, vol. 110, no. 4, Aug. 2011, Art. no. 044506.
- [13] R. Ge et al., "Atomristor: Nonvolatile resistance switching in atomic sheets of transition metal dichalcogenides," *Nano Lett.*, vol. 18, pp. 434–441, Jan. 2018.
- [14] Y. Huang et al., "2D RRAM and Verilog-A model for Neuromorphic Computing," in *Proc. IEEE 16th Nanotechnol. Mater. Devices Conf.* (NMDC), Dec. 2021, pp. 1–4.
- [15] X. Wu et al., "Thinnest nonvolatile memory based on monolayer h-BN," Adv. Mater., vol. 31, no. 15, Apr. 2019, Art. no. 1806790.
- [16] R. Ge et al., "A library of atomically thin 2D materials featuring the conductive-point resistive switching phenomenon," *Adv. Mater.*, vol. 33, no. 7, Feb. 2021, Art. no. 2007792.
- [17] W. Banerjee, "Challenges and applications of emerging nonvolatile memory devices," *Electronics*, vol. 9, no. 6, p. 1029, 2020.
- [18] H. Yang et al., "Two-dimensional materials prospects for non-volatile spintronic memories," *Nature*, vol. 606, no. 7915, pp. 663–673, Jun. 2022.

- [19] Y. Huang, X. Wu, Y. Gu, R. Ge, D. Akinwande, and J. C. Lee, "On the stochastic nature of conductive points formation and their effects on reliability of MoS₂ RRAM: Experimental characterization and Monte Carlo simulation," *Microelectron. Rel.*, vol. 126, Nov. 2021, Art. no. 114274.
- [20] Y. Gu et al., "Sulfurization engineering of one-step low-temperature MoS₂ and WS₂ thin films for memristor device applications," Adv. Electron. Mater., vol. 8, no. 2, Feb. 2022, Art. no. 2100515.
- [21] J. Di, J. Du, Z. Lin, S. Liu, J. Ouyang, and J. Chang, "Recent advances in resistive random access memory based on lead halide perovskite," *InfoMat*, vol. 3, no. 3, pp. 293–315, Mar. 2021.
- [22] C. Pan et al., "Coexistence of grain-boundaries-assisted bipolar and threshold resistive switching in multilayer hexagonal boron nitride," Adv. Funct. Mater., vol. 27, no. 10, 2017, Art. no. 1604811.
- [23] Z. Zhang et al., "Memory materials and devices: From concept to application," *InfoMat*, vol. 2, no. 2, pp. 261–290, Mar. 2020.
- [24] R. Ge et al., "Atomristors: Memory effect in atomically-thin sheets and record RF switches," in *IEDM Tech. Dig.*, 2018, p. 22.
- [25] X. Wu et al., "Electron irradiation-induced defects for reliability improvement in monolayer MoS2-based conductive-point memory devices," npj 2D Mater. Appl., vol. 6, no. 1, pp. 1–12, May 2022.
- [26] M. S. Liao and W. H. E. Schwarz, "Effective radii of the monovalent coin metals," *Acta Crystallographica Sect. B, Struct. Sci.*, vol. 50, no. 1, pp. 9–12, Feb. 1994.
- [27] S. M. Hus et al., "Observation of single-defect memristor in an MoS₂ atomic sheet," *Nature Nanotechnol.*, vol. 16, no. 1, pp. 58–62, Jan. 2021.
- [28] X. Guan, S. Yu, and H.-S. P. Wong, "On the switching parameter variation of metal-oxide RRAM—Part I: Physical modeling and simulation methodology," *IEEE Trans. Electron Devices*, vol. 59, no. 4, pp. 1172–1182, Apr. 2012.
- [29] S. Yu, X. Guan, and H.-S. P. Wong, "On the stochastic nature of resistive switching in metal oxide RRAM: Physical modeling, Monte Carlo simulation, and experimental characterization," in *IEDM Tech. Dig.*, 2011, p. 17.